Interpretation of segmental orientation in deformed networks in terms of constrained junction model of rubber elasticity

B. Erman and I. Bahar
Polymer Research Center and School of Engineering, Bogazici University, Bebek 80815, Istanbul, Turkey

and S. Besbes, L. Bokobza* and L. Monnerie
Laboratoire de Physico-Chimie Structurale et Macromoléculaire, ESPCI, 10 rue Vauquelin, 75231 Paris Cédex 05, France
(Received 21 May 1992; revised 30 July 1992)

Results of Fourier transform infra-red (*FT*i.r.) dichroism measurements of segmental orientation in model poly(dimethylsiloxane) (PDMS) networks of different molecular weights between junctions are interpreted in terms of the constrained junction model of rubber elasticity. The theory shows quantitative agreement with experimental data, without the necessity of adjusting any parameter. Based on this agreement, one may conclude that in PDMS networks, the dependence of orientation on deformation results from the non-affine transformation of junction points, and that local intermolecular contributions to segmental orientation are not significant. In the case of less flexible chains such as polyisoprene on the other hand, intermolecular contributions to segmental orientation might be relatively more important. Correspondence between birefringence experiments and segmental orientation is formulated which permits direct quantitative comparison between the birefringence and *FT*i.r. dichroism experiments.

(Keywords: poly(dimethylsiloxane) networks; segmental orientation; *FT*i.r. measurements; constrained junction theory of rubber elasticity)

INTRODUCTION

Recently we have reported results of Fourier transform infra-red (*FT*i.r.) dichroism measurements of segmental orientation in well characterized poly(dimethylsiloxane) (PDMS) networks formed by end-linking[1]. The values of segmental orientation were obtained in five networks of different molecular weights M_c between junctions, ranging from 2000 to 23 000. The measured values of orientation were found to lie between the predictions of the phantom and affine network models. It was suggested[1] that this behaviour was similar to that from the predictions of the constrained junction or the constrained chain models[2] but a detailed analysis was not presented. In the present paper, we interpret the results of the *FT*i.r. segmental orientation measurements in terms of the constrained junction theory of amorphous elastomeric networks. This presentation is prompted by a recent paper by Brereton[3] suggesting that the doublet structure observed in ^{2}H n.m.r. experiments of Sotta and Deloche[4] on segmental orientation in PDMS networks results from the strain dependence of the fluctuations of junction points in networks. The molecular mechanisms contributing to segmental orientation considered by Brereton have been incorporated[5], in great detail, into the model of a network that exhibits deviations from the classical phantom network model. The predictions of this theory, as well as of a previous similar treatment of segmental orientation in terms of strain birefringence[6], showed satisfactory agreement with experimental data on various elastomeric systems[7,8] obtained by different experimental techniques. The strain dependence of segmental orientation and birefringence observed in all of the experiments closely followed the predictions of the constrained junction model of amorphous networks[9,10]. A precise theoretical model describing the state of deformation and segmental orientation in network chains seems to be of particular importance at the present time when higher resolution and precision is provided by advanced spectroscopic techniques such as ^{2}H n.m.r., two-dimensional i.r.[11] and modulated *FT*i.r.[12] in determining segmental orientation. The present interpretation of segmental orientation of PDMS in terms of the constrained junction model and the discussion of factors affecting this phenomenon is an attempt along this direction.

The fact that experimental values[1] of segmental orientation in PDMS networks are in quantitative agreement with predictions from the molecular theory based on the specific structural features of the chains is an improvement over previous treatments of segmental orientation which have been based on the affinely deforming chain and the acceptance of the Kuhn length. For this reason, a large portion of the present paper is

* To whom correspondence should be addressed

0032-3861/93/091858-07

devoted to a review of recent developments in the theory of segmental orientation. The agreement and disagreement between theory and the present data for PDMS are discussed critically. In the final section, segmental orientation is related to strain induced birefringence in networks, and factors affecting the governing parameters are discussed.

APPLICATION OF THE CONSTRAINED JUNCTION MODEL TO SEGMENTAL ORIENTATION IN PDMS NETWORKS

Comparison of the phantom and affine model predictions with experimental results

The orientation function S for segmental orientation in phantom and affine network models under uniaxial extension is written in terms of the extension ratio λ as:

$$S_{\text{phantom}} = D_0(1-2/\phi)(\lambda^2-\lambda^{-1}) = D_0(1-2/\phi)(v_{2c}/v_2)^{2/3}(\alpha^2-\alpha^{-1})$$
$$S_{\text{affine}} = D_0(\lambda^2-\lambda^{-1}) = D_0(v_{2c}/v_2)^{2/3}(\alpha^2-\alpha^{-1}) \quad (1)$$

where λ is defined as the ratio of the final length of the network in the direction of stretch to the length in the state of reference obtained during the formation of the network. α is the ratio of the final length to the initial, undistorted length. In the case of samples swollen prior to deformation, the initial length is that of the swollen state. v_{2c} and v_2 have their usual meanings as the volume fraction of polymer during crosslinking and during the stretching experiment, respectively. ϕ is the functionality of junctions and D_0 is the configurational factor given by the theory in the Nagai formulation for affine networks as[2,13]:

$$D_0 = (3\langle r^2\cos^2\Phi\rangle_0/\langle r^2\rangle_0 - 1)/10 \quad (2)$$

Here, Φ is the angle between a unit directional vector $\mathbf{u}_0$ affixed to a chain segment whose orientation is being considered and the chain end-to-end vector $\mathbf{r}$. The angular brackets denote the ensemble average and the subscript zero indicates that averaging is performed for chains in the unconstrained state. Defined in this manner, the parameter D_0 reflects the intrinsic orientational behaviour of a single chain which is not subject to any orientational correlations with the spatially neighbouring chains. Both in the phantom and the affine network models, the chains are assumed to be free of any intermolecular effects. The difference of the two expressions in equation (1) arises from the difference of the state of deformation at the molecular level in the phantom and the affine models.

For convenience, the data is usually presented in terms of the reduced orientation function $[S]$ by dividing the second and fourth terms in equation (1) by $(v_{2c}/v_2)^{2/3}(\alpha^2-1/\alpha)$ as:

$$[S] \equiv \frac{S}{(v_{2c}/v_2)^{2/3}(\alpha^2-\alpha^{-1})} = \begin{cases}(1-2/\phi)D_0 & \text{Phantom}\\ D_0 & \text{Affine}\end{cases} \quad (3)$$

This operation removes the deformation and swelling dependence of the data. The new variable $[S]$ is a function of D_0 and junction functionality only. In the affine network, the junctions are embedded in their surroundings and are fully affected by the macroscopic strain. In the phantom network model, the junctions are allowed to fluctuate, with amplitudes depending on the network topology as indicated by the junction functionality. The deformation at the molecular level and therefore the segmental orientation are less affected by macroscopic strain.

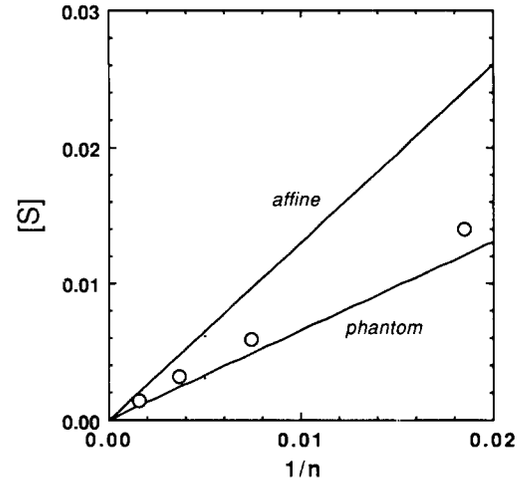

Figure 1 Dependence of the configurational factor D_0 on chain length. Points represent results from *FT*i.r. experiments from reference 1, with dry PDMS networks. The two curves represent the affine and phantom network limits obtained with the use of the RIS formalism

According to the theory[14], D_0 varies as the inverse of the number of bonds n in the chain between two junctions. Thus, a plot of the reduced orientation function as a function of n^{-1} gives a straight line as shown in *Figure 1*. Both lines are drawn by using equation (3) for a tetrafunctional PDMS network with the proper value of D_0 obtained from the previous rotational isomeric state (RIS) calculations[1]. Here, D_0 is representative of the orientation of vectors along consecutive oxygen atoms. The points represent results of *FT*i.r. experiments on end-linked PDMS networks obtained previously[1] from the slopes of the straight lines passing through S *versus* λ^2-1/λ points. The experimental data represent, like the calculations, the orientation of vectors along the consecutive oxygen bonds[15]*. The occurrence of the experimental points between the affine and the phantom network predictions indicates that the state of deformation at the molecular level is intermediate between those in the phantom and the affine network models. This conclusion is in agreement with the predictions of the constrained junction model for segmental orientation. In the next section, we briefly review the molecular aspects of the constrained junction model.

Summary of the constrained junction model and application to segmental orientation

The detailed picture of the constrained junction model of amorphous networks follows from the work of Flory[9] according to which intermolecular contributions are represented in the form of spring-like constraints hindering the fluctuations of junctions. These constraints

* *FT*i.r. experiments measure the orientation of the vector bisecting the CH_3–Si–CH_3 bond. Passage to the orientation of the vector along the O–O direction is made by the expression:

$$[S] = \frac{R-1}{R+2}\frac{2}{(3\cos^2\beta-1)}$$

where β is the angle ($=90°$) between the two directions stated above

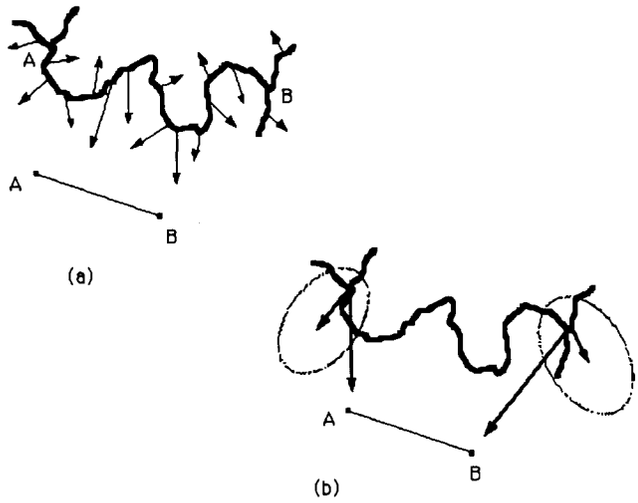

Figure 2 (a) Schematic representation of a network chain between two junction points A and B. Thick and thin curves represent the instantaneous configuration of a real chain and that of a phantom model chain, respectively. Arrows indicate the constraints from the surroundings. (b) Constrained junction chain in which the action from the surroundings is concentrated at the junctions only. Junctions fluctuate within the indicated elliptic domains referred to as the constraint domains

are assumed to result from entanglements among chains in the connected network structure. In the absence of connectivity, they are expected to vanish. The fact that such intermolecular effects are concentrated at the junctions is of mathematical convenience. A later treatment[16], referred to as the constrained chain model, assumed the constraints to operate directly on the chains. The general features of rubber elasticity and birefringence predicted by this model are qualitatively similar to those of the constrained junction model[16,17].

A somewhat pictorial representation of an entangled chain AB in a network is shown in *Figure 2a*. The line AB indicates the time average location of the chain ends as would be obtained in the phantom network. The thick curve is representative of an instantaneous configuration of the chain. The excursion of the chain to positions away from the requirements of the phantom network in the deformed state results in the 'spring-like' reactions of the neighbouring chains as shown by the various arrows in the figure. These are intermolecular forces absent in the phantom and the affine network models. In *Figure 2b*, these forces are concentrated on the junctions only. Each junction is assumed to be under the action of two forces: (1) the intramolecular elastic force from the network connectivity, trying to restore the junction to its mean position as obtained in the phantom network; and (2) another spring-like force arising from the distortions of the surroundings, trying to restore the junction to a point referred to as the centre of constraints. In the absence of constraints, the junction fluctuates in a spherical domain with an average squared radius of $\langle \Delta R^2 \rangle_0 = [(\phi-1)/\phi(\phi-2)]\ \langle r^2 \rangle_0$ which is independent of macroscopic strain[9]. In the absence of network connectivity, the junction is assumed to fluctuate in a region referred to as the constraint domain. The macroscopic strain is assumed to deform the constraint domains affinely. The two ellipses at the extremities of the network chain in *Figure 2b* are drawn to indicate the spatial range of constraint domains. The distortion of the surroundings results in a further orientation in the domain.

The strength of the constraints varies inversely with the size of the constraint domain. Infinitely strong constraints do not permit fluctuations of the junction at all and the junctions are securely embedded in their environments. This extreme case represents the affine network model. The strength of the constraints diminishes as the constraint domain enlarges. As the network is stretched, the constraint domains deform into ellipses and their effect on the junction becomes more anisotropic. The strength of intermolecular constraints in the undeformed network is represented in the theory by the parameter κ defined as:

$$\kappa = \frac{\langle \Delta R^2 \rangle_0}{\langle \Delta s^2 \rangle_0} \tag{4}$$

where the numerator and the denominator represent the mean square radii of fluctuation domain of the junction in the phantom network and the constraint domain, respectively[9,10]. In terms of the molecular weight, M_c, between junctions and v_{2c}, κ is given by the relation:

$$\kappa = C M_c^{1/2} v_{2c} \tag{5}$$

with the proportionality constant $C \approx 0.07$ obtained from previous data on PDMS networks[8,18].

In the constrained junction model, the mean squared extension ratio, Λ_t^2 at the molecular level along the direction t reads[6]:

$$\Lambda_t^2 = (1-2/\phi)\lambda_t^2 + (2/\phi)(1+B_t) \qquad t = x, y, z \tag{6}$$

where B_t is

$$B_t = \kappa^2(\lambda_t^2 - 1)/(\kappa + \lambda_t^2)^2 \qquad t = x, y, z \tag{7}$$

The orientation of chain segments results from the anisotropy of deformation at the molecular level. The orientational field resulting from the anisotropic distortion of the constraint domains may further induce an orientation, as has been previously suggested[6]. Accordingly, the distortion of the constraint domains is described by the three quantities:

$$\Theta_t^2 = 1 + \lambda_t^2 B_t/\kappa \qquad t = x, y, z \tag{8}$$

In uniaxial tension the state of segmental orientation is described by the two expressions[5]:

$$S' = D_0[\Lambda_x^2 - (\Lambda_y^2 + \Lambda_z^2)/2]$$
$$S'' = eD_0[\Theta_x^2 - (\Theta_y^2 + \Theta_z^2)/2] \tag{9}$$

Here, the coefficient e is adopted to represent the strength of the local orientational field arising from the distortions of the constraint domains. The total orientation is the sum of S' and S''. Using equations (6), (8) and (9), the reduced orientation defined by equation (3) for uniaxial extension is written in the following form:

$$[S] = (1-2/\phi)D_0\left\{1 + \frac{(v_2/v_{2c})^{2/3}}{(\phi/2-1)(\alpha^2-\alpha^{-1})}[B_x - B_y + (\phi e/2\kappa)(\lambda_x^2 B_x - \lambda_y^2 B_y)]\right\} \tag{10}$$

When $\kappa = 0$, as B_t scales with κ^2 for small κ, the term in square brackets on the right-hand side of equation (10) becomes zero and the reduced orientation for the phantom network model is recovered. The term in square brackets also goes to zero as α increases indefinitely.

Comparison of experimental data and the constrained junction model predictions

Results of experiments on samples A and B in *Table 1*, with respective molecular weights $M_c = 12\,000$ (open symbols) and 23 000 (closed symbols) are shown in *Figure 3*. In this figure, the reduced orientation is presented as a function of α^{-1}. Experimental points at lower values of α showed excessive scatter and are therefore not included. The straight lines are least squares fits to the points. The curves are calculated from equation (10) with the values of the parameters listed in *Table 1*. The tendency of $[S]$ values to decrease with increasing α is clearly seen. This feature is also seen in the birefringence data of reference 8. It is interesting to note that the α^{-1} intercepts of the straight lines in *Figure 3* meet with the intercepts of the theoretical curves obtained from RIS calculations[1]. It should be noted that the values for κ and e in *Table 1* follow from previous experimental data[8], thus the theory contains no adjustable parameters. The experimental points and theory tend to diverge at smaller values of α. The theoretical curves level off as $\alpha = 1$ is approached while the experimental $[S]$ values increase, exhibiting a Mooney–Rivlin type behaviour. The largest discrepancy between the theory and the straight lines through the data is at $\alpha = 1$ and amounts to 25 and 26% for samples A and B, respectively.

Table 1 Values of parameters used in the calculations of orientation from equation (10)

Sample	M_c	κ^a	$[S]_{ph}{}^b$	e^c
A	23 000	10.7	0.001045	0.5
B	12 000	7.7	0.002000	0.5
C	10 000	7.0	0.002405	0.5
D	2000	3.1	0.012025	0.0
E[d]	7600	5.5	0.004050	0.5

[a] Calculated from equation (5)
[b] Obtained from RIS calculations[1] of D_0
[c] The value of 0.5 was obtained in previous work[8] on stress–strain isotherms of PDMS
[d] From birefringence data[8]
The networks were tetrafunctional, $\phi = 4$. Crosslinking and measurements were performed in the bulk state for all samples. Results[28] for the network with $M_c = 5000$ have not been included because of excessive scatter in the data

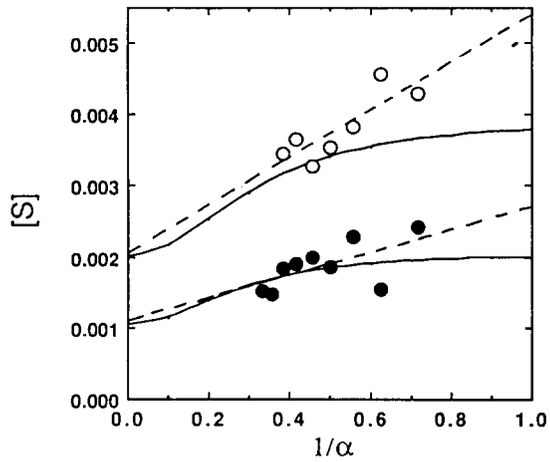

Figure 3 Reduced orientation $[S]$ as a function of α^{-1}. Open and closed circles represent the experimental data for dry PDMS network chains of $M_c = 12\,000$ and 23 000, respectively. Curves result from the constrained junction model, using the variables listed in *Table 1*. Best fitting straight lines through the experimental data are also shown (broken line)

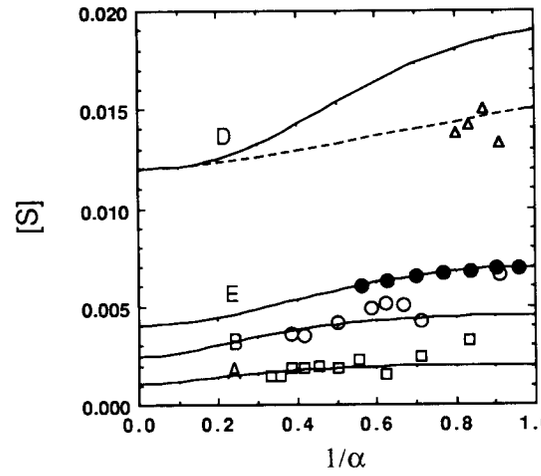

Figure 4 Reduced orientation $[S]$ as a function of α^{-1}. Open triangles, circles and squares are the experimental data for dry networks with $M_c = 2000$, 10 000 and 23 000 as labelled in the figure. The solid circles represent results of birefringence experiments with $M_c = 7600$. Curves are obtained with the constrained junction model, using the variables listed in *Table 1*. The broken curve is obtained for sample D using $\kappa = 1$

Predictions of the constrained junction model and experimental data are further compared in *Figure 4*. The open triangles, circles and squares are from *FT*i.r. dichroism experiments[1] for the respective networks with $M_c = 2000$, 10 000 and 23 000 as labelled in the figure. The closed circles represent results of birefringence experiments. The birefringence data are multiplied by a proportionality constant inasmuch as birefringence and orientation are related by a constant coefficient as described in detail below.

The parameters used in the calculation of the curves according to equation (10) are given in *Table 1*. Except for the value $e = 0$ for sample D, no parameter is adjusted in the calculations. The maximum discrepancy between theory and experiment is for sample D with the smallest M_c. The curve is calculated from theory with $\kappa = 3.1$ resulting from equation (5). The theoretical prediction for $[S]$ is ~26% higher than the experimental value at $\alpha = 1$. It is calculated that the choice of $\kappa = 1.0$ instead of 3.1 leads to a good agreement with experiments, as shown by the broken curve in *Figure 4*. This observation is in line with results of computer simulations by Adolf and Curro[19] where a stronger dependence of κ on M_c is predicted instead of that given by equation (5).

The curve obtained from birefringence experiments in *Figure 4* closely agrees with the deformation dependence expected from equation (10). The agreement is much better than that of the *FT*i.r. data, most probably due to large scatter in the latter. A possible source of the difference between birefringence and *FT*i.r. results may be due to the procedures in measuring the deformation. The birefringence data were obtained by the successive application of dead weights to the sample and measuring changes in length. The measurements in *FT*i.r. were made by keeping the two ends of the sample fixed at specified distances. Furthermore, orientation measurements in *FT*i.r. required rotation of the stretched sample parallel and perpendicular to the direction of polarization of the light source.

INTRA- AND INTERMOLECULAR CONTRIBUTIONS TO SEGMENTAL ORIENTATION

Orientation of segments in a real network differs from that in the phantom model in two respects, according to equation (10). First, the chains in the real network deform more than those in the phantom model depending on the magnitude of the κ parameter. Secondly, segments experience a local orientation field resulting from the distortion of the constraint domains. The latter is introduced into the theory in an *ad hoc* manner by the coupling parameter e in equation (10). In addition to these two sources of orientation, there may exist local interchain interactions among neighbouring segments. Such interactions exist inherently due to the linear connectivity of the chains, in the network as well as in the bulk state, and result in the enhancement of segmental orientations[20]. In previous work[5,21,22], this type of intermolecular interaction has been attributed to the tendency of two neighbouring segments to align as obtained in nematic liquid crystalline systems. Recent treatment of networks by a lattice model[23,24] shows that such nematic-like interactions exist in semiflexible chains with relatively large length-to-width ratios of their Kuhn segments. Such interactions are therefore specific to the system and should be negligible in highly flexible chains such as PDMS. In any case, their action may be brought into the theory[5] by allowing for the distortion of the unit vector $\mathbf{u}_0$ of the isolated chains by an amount $\Delta\mathbf{u}$ such that the modified configurational factor D becomes:

$$D=\{3\langle[\mathbf{r}_0(\mathbf{u}_0+\Delta\mathbf{u})]^2\rangle_0/\langle r^2\rangle_0-1\}/10$$
$$=D_0+3\langle\Delta\mathbf{u}^2\cos^2\delta\rangle/10\equiv D_0+D_{\text{int}} \quad (11)$$

Here δ is the angle between $\Delta\mathbf{u}$ and $\mathbf{r}$. The intermolecular contribution D_{int} is, according to Jarry and Monnerie[21]:

$$D_{\text{int}}=\frac{V}{1-V}D_0 \quad (12)$$

Here, V reflects the intensity of interactions between orientations of neighbouring segments. According to the lattice model[23,24] V equates to:

$$V=\frac{1}{(64/5x)(1-x/x_a)+1}+\frac{\tilde{T}^{-1}}{5} \quad (13)$$

Here, $\tilde{T}$ is the reduced temperature accounting for the strength of the nematic interactions, x is the length-to-width ratio of Kuhn segments composing the network chains and x_a is the critical value of x above which the unperturbed system is totally anisotropic. The intermolecular contribution is expected to vanish readily by swelling the network with a suitable solvent.

A further contribution to orientation due to trapped entanglements has been suggested by Herz *et al.*[25] and Deloche *et al.*[26,27]. According to their theory, such contributions persist even in the swollen network, but their effects should vanish if the networks are originally formed in the highly diluted state. One may therefore separate the contributions from intermolecular sources into a local and an entanglement component and rewrite equation (11) in the following form as a first approximation:

$$D=D_0+D_1v_2+D_2v_{2c} \quad (14)$$

Here, D_1 reflects the contributions from local intermolecular correlations and D_2 is due to the field induced by trapped entanglements. Strong contributions from D_1 have been reported previously[7] for the orientation of polyisoprene (PIP) networks by polarized fluorescence measurements. Results of *FT*i.r. experiments on swollen PDMS networks reported in the paper[28] show however that D_1 is not significant for this system. The effects of swelling on segmental orientation are compared in *Figure 5* for PIP and PDMS networks. The upper set of solid points show results of measurements on a dry PIP network. The curve through the points is obtained according to the constrained junction model[7]. Results for the network in the swollen state with $v_2=0.88$ and 0.81, are shown by the open circles and triangles, respectively. A very strong decrease in $[S]$ is obtained by small amounts of swelling as seen in the figure. The theoretical curves obtained with $v_2=0.88$ and 0.81 showed imperceptible differences from that of the dry network. It was not therefore possible to fit a theoretical curve through the data for $v_2\neq 1$ without modifying the front parameter D. The two curves through the data points for the swollen samples in *Figure 5* are obtained by choosing $D=0.008$ and 0.0066 for $v_2=0.88$ and 0.81, respectively. This decrease in D may be attributed to the disappearance of intermolecular effects upon swelling, as delineated in equation (14). The lowest curve and the corresponding data points are obtained for the PDMS network[28] B with $v_2=1$ and 0.56. The differences between the two data sets are not discernible in the figure in parallel with the predictions of the constrained junction model. This indicates that intermolecular contributions to the configurational factor D are negligible in PDMS networks.

In *Figure 6*, the effect of v_{2c} on segmental orientation in PDMS networks is shown[28]. Solid circles are obtained for sample B formed at $v_{2c}=1.0$. The open circles are for the network formed at $v_{2c}=0.7$. The best fitting straight lines through the data points are also shown. The curve is obtained from the constrained junction model for both $v_{2c}=1.0$ and 0.7. While the theory predicts no effect on reduced segmental orientation from dilution during formation, the experimental data show some decrease.

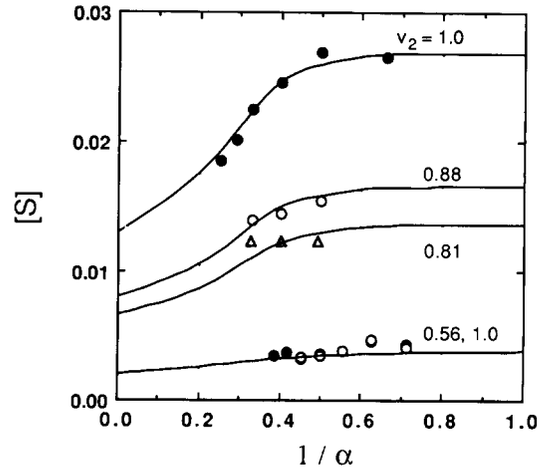

Figure 5 Effect of swelling on segmental orientation of deformed PIP and PDMS networks. The three upper sets of experimental data are for PIP networks with the indicated volume fractions v_2 during deformation. The data points on the lowest curve are measured for PDMS networks with $v_2=1.0$ (solid circles) and 0.56 (open circles). The two curves for $v_2=1.0$ are obtained from the constrained junction theory with no adjustable parameters. The intermediate curves necessitated readjustment of the front parameter D to account for intermolecular effects

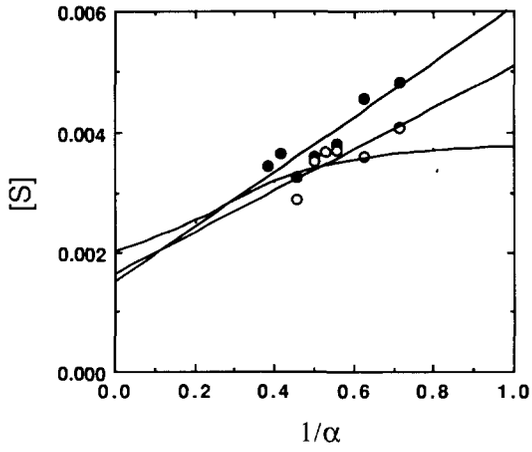

Figure 6 Effect of v_{2c} on segmental orientation in PDMS. The solid and open circles represent [S] values measured for the respective values of $v_{2c}=1.0$ and 0.7. Best fitting straight lines and the theoretical curve from the constraint junction model are also displayed

The magnitude of the decrease, however, is within experimental error bounds.

The absence of contributions from D_1 and D_2 terms to the configuration factor D in PDMS networks justifies the close agreement between measured orientations and the RIS calculations performed in previous work[1].

RELATIONSHIP BETWEEN SEGMENTAL ORIENTATION AND STRAIN BIREFRINGENCE

Correspondence between the reduced birefringence and reduced orientation function

Measurement of strain birefringence of deformed networks is an alternative technique for determining the degree of orientation of chain segments. This technique detects the changes in the components of the polarizability tensor of chain units under deformation. As will be shown in this section, these changes may be related, quantitatively, to the configurational factor D_0 introduced above for characterizing segmental orientation.

In *FT*i.r. experiments, the orientation of a specific direction rigidly affixed to the chain is measured directly. The components of the polarizability tensor, on the other hand, include contributions from segments neighbouring a chosen segment. In the bulk state, mutual alignment of neighbouring segments therefore contributes to the measured birefringence. Thus, this technique is very sensitive to intermolecular effects, and its correspondence to *FT*i.r. experiments can be made only in the highly diluted state of the network where the chains are sufficiently separated from each other. Another requirement for comparison is that the diluent should be isotropic inasmuch as a slight anisotropy of the solvent molecules will superpose on the optical anisotropy tensor of the chain units.

Experimentally[8], the difference $\Delta n_{xy}=n_x-n_y$ in the refractive index of a stretched sample along the direction of stretch x and the lateral direction y is measured. According to theory, the reduced birefringence $[\Delta n_{xy}]$ is given by the expression[6]:

$$[\Delta n_{xy}]\equiv\frac{\Delta n_{xy}(v_2/v_{2c})^{1/3}}{(\alpha^2-\alpha^{-1})}$$

$$=(1-2/\phi)\frac{vkT}{V_0}C\left\{1+\frac{(v_2/v_{2c})^{2/3}}{(\phi/2-1)(\alpha^2-\alpha^{-1})}\times[B_x-B_y+(\phi e/2\kappa)(\lambda_x^2B_x-\lambda_y^2B_y)]\right\} \quad (15)$$

where v/V_0 is the number of chains per unit volume in the reference state, k is the Boltzmann constant, T is the absolute temperature and C is the stress-optical coefficient given by:

$$C=2\pi(\bar{n}^2+2)^2\Gamma_2^0/27\bar{n}kT \quad (16)$$

Here, $\bar{n}$ is the mean refractive index of the network and Γ_2^0 refers to the intrinsic optical anisotropy of a given chain. The superscript zero indicates that the optical anisotropy is obtained in the absence of intermolecular interactions, i.e. in the state swollen with an isotropic solvent.

The expression in braces on the right-hand side of equation (15) is identical to the reduced orientation expression given by equation (10). Accordingly, the experimental data available for the reduced birefringence $[\Delta n_{xy}]$ may be transformed into [S] by using the simple relationship:

$$[S]=\frac{D_0}{CvkT/V_0}[\Delta n_{xy}] \quad (17)$$

In the limit as α^{-1} approaches zero, $[\Delta n_{xy}]$ assumes its phantom network limiting value:

$$[\Delta n_{xy}]_{\text{phantom}}=(1-2/\phi)\frac{vkT}{V_0}C \quad (18)$$

which provides a direct method of evaluating the factor $CvkT/V_0$ appearing in the denominator of equation (17). It is noted from equations (17) and (18) that the phantom network limit $[S]_{\text{phantom}}$ which is given by equation (3), is recovered by extrapolating the [S] results to $\alpha^{-1}=0$.

Relationship between the optical anisotropy Γ_2^0 and the configurational factor D_0 for PDMS

From molecular considerations Γ_2^0 is expressed in terms of the anisotropic part $\hat{\alpha}_i$ of the polarizability tensor of the structural units of the chain as[8]*:

$$\Gamma_2^0=\frac{9}{10}\sum_i\langle\mathbf{r}^{\mathrm{T}}\hat{\alpha}_i\mathbf{r}\rangle_0/\langle r^2\rangle_0 \quad (19)$$

The anisotropic part of the polarizability tensor may be defined with respect to a coordinate system xyz, affixed to the repeat unit of the PDMS chain. At a given configuration of the chain, the angles between the x, y and z axes of the ith unit and the chain vector are defined, respectively, by ϕ_{ix}, ϕ_{iy}, ϕ_{iz}. In the approximation of tetrahedral symmetry about Si and C atoms, selecting the x-axis along the O...O direction, the y-axis perpendicular to it, in the plane of the Si-O bond and the z-axis parallel to $CH_3...CH_3$, $\hat{\alpha}_i$ for each of the dimethylsiloxane structural units $1\leqslant i\leqslant n/2$ in a PDMS chain of n backbone bonds is:

$$\hat{\alpha}_i=\Delta\alpha\,\mathrm{diag}(2/3,\ 0,\ -2/3) \quad (20)$$

where $\Delta\alpha$ is estimated[8] for PDMS to be equal to 0.018 Å^3.

* The symbol α is retained for the polarizability tensor to conform with the conventional notation in literature and should not be confused with the scalar α representing the stretch ratio

Equation (19) may be written in terms of the angles ϕ_{ix}, ϕ_{iy}, ϕ_{iz} by projecting the tensor $\hat{\alpha}_i$ along the end-to-end vector as:

$$\Gamma_2^0 = \frac{3}{5}\frac{\Delta\alpha}{\langle r^2\rangle_0}\sum_i(\langle r^2\cos^2\phi_{ix}\rangle - \langle r^2 cos^2\phi_{iz}\rangle) \quad (21)$$

Upon rearrangement, equation (21) reduces to:

$$\Gamma_2^0 = n\,\Delta\alpha[D_{0,\parallel} - D_{0,\perp}] = 3n\,\Delta\alpha D_0 \quad (22)$$

Here $D_{0,\parallel}$ and $D_{0,\perp}$ refer to the orientational configurational factors associated with the vectors along the O...O direction and perpendicular to it, respectively. Inasmuch as i.r. dichroism experiments[15] measure the orientation of vectors along the O...O direction, $D_{0,\parallel}$ is identical to D_0 and $D_{0,\perp}$ is equal to $-2D_0$.

Comparison with experiments

Birefringence experiments performed with PDMS networks of $M_c = 7600$ in optically isotropic diluents yield[8] $\Gamma_2^0 = 0.04\,\text{Å}^3$ with carbon tetrachloride and $\Gamma_2^0 = 0.14\,\text{Å}^3$ with tetraethyl methane. These values are much smaller than those measured in the bulk state or in the state swollen with anisotropic solvents. Adopting the mean value for Γ_2^0 from the two experiments, as suggested previously[8], we obtain from equation (22), $D_0 = 0.0081$. It is noted that the configurational factor for a chain of $M_c = 7600$ is obtained as[1] $D_0 = 0.0063$ from RIS calculations, which is in reasonable agreement with the result of 0.0081 deduced from birefringence data.

According to equations (17) and (18), the quantitative passage from $[\Delta n_{xy}]$ *versus* α^{-1} curves of reference 8 to $[S]$ as a function of α^{-1} is readily done by dividing the $[\Delta n_{xy}]$ values by their α^{-1} intercept, and multiplying by $(1-2/\phi)D_0$. This procedure has been adopted for plotting the solid circles in *Figure 4*. The theoretical curve E has been drawn by using the parameters listed in *Table 1*.

CONCLUSIONS

The following conclusions can be drawn from the present study.

1. In general, segmental orientation for PDMS from *FT*i.r. measurements is in agreement with RIS predictions. Compared to all previous theoretical work, which is based on the hypothetical Kuhn segment model, the RIS formalism appears as a quantitatively more realistic approach.
2. The experimentally observed strain dependence of the reduced orientation which cannot be explained by either affine or phantom network models, is suitably accounted for by the constrained junction model of rubber elasticity.
3. The weak dependence of segmental orientation on the state of swelling during both network formation and measurements conforms with the front factor $(v_{2c}/v_2)^{2/3}$ as delineated in equation (1).
4. The agreement between theory and experiments is poorer with decreasing M_c, which may be attributed to the inadequacy of equation (5) to evaluate the parameter κ at high crosslinking densities, as previously pointed out by Adolf and Curro[19].
5. Birefringence measurements of networks swollen with optically isotropic diluents may be readily employed to estimate segmental orientation and may be interpreted with the same mathematical formulation, as presented above.
6. Measurements of orientation in PIP networks indicate that local intermolecular contributions to orientation are significant as demonstrated by the rapid decrease in $[S]$ with swelling, in contrast to PDMS networks. This brings into consideration the existence of stronger intermolecular effects on segmental orientation in less flexible chains.

ACKNOWLEDGEMENT

This work was supported by the NATO grant no. CRG 910422.

REFERENCES

1 Besbes, S., Cermelli, I., Bokobza, L., Monnerie, L., Bahar, I., Erman, B. and Herz, J. *Macromolecules* 1992, **25**, 1949
2 Mark, J. E. and Erman, B. 'Rubberlike Elasticity: A Molecular Primer', Wiley Interscience, New York, 1988
3 Brereton, M. G. *Macromolecules* 1991, **24**, 6160
4 Sotta, P. and Deloche, B. *Macromolecules* 1990, **23**, 1999
5 Erman, B. and Monnerie, L. *Macromolecules* 1985, **18**, 1985
6 Erman, B. and Flory, P. J. *Macromolecules* 1983, **16**, 1601
7 Queslel, J. P., Erman, B. and Monnerie, L. *Macromolecules* 1985, **18**, 1991
8 Erman, B. and Flory, P. J. *Macromolecules* 1983, **16**, 1607
9 Flory, P. J. *J. Phys. Chem.* 1977, **66**, 5720
10 Flory, P. J. and Erman, B. *Macromolecules* 1982, **15**, 800
11 Noda, I. *Appl. Spectrosc.* 1990, **4**, 550
12 Bokobza, L. and Monnerie, L. work in progress
13 Nagai, K. *J. Chem. Phys.* 1964, **40**, 2818
14 Erman, B. and Bahar, I. *Macromolecules* 1988, **21**, 452
15 Monnerie, L. *Faraday Symp. Chem. Soc.* 1983, **18**, 1
16 Erman, B. and Monnerie, L. *Macromolecules* 1987, **22**, 3347
17 Galiatsatos, V. *Comput. Polym. Sci.* 1991, **1**, 51
18 Queslel, J. P. personal communication
19 Adolf, D. B. and Curro, J. G. *Macromolecules* 1987, **20**, 1646
20 Flory, P. J. *Faraday Discuss. R. Soc. Chem.* 1979, **68**, 14
21 Jarry, J. P. and Monnerie, L. *Macromolecules* 1979, **12**, 316
22 Deloche, B. and Samulski, E. T. *Macromolecules* 1981, **14**, 575
23 Erman, B., Bahar, I., Kloczkowski, A. and Mark, J. E. *Macromolecules* 1990, **23**, 5335
24 Bahar, I., Erman, B., Kloczkowski, A. and Mark, J. E. *Macromolecules* 1990, **23**, 5341
25 Herz, J., Munch, J. P. and Candau, S. *J. Macromol. Sci. Phys.* 1980, **B18**(2), 267
26 Dubault, A., Deloche, B. and Herz, J. *Macromolecules* 1987, **20**, 2096
27 Sotta, P., Deloche, B., Herz, J., Lapp, A., Durand, D. and Rabadeux, J.-C. *Macromolecules* 1987, **20**, 2769
28 Besbes, S., Bokobza, L., Monnerie, L., Bahar, I. and Erman, B. *Polymer* in press